Journal of Chromatography A, 1217 (2010) 1942–1949

Contents lists available at ScienceDirect

Journal of Chromatography A

journal homepage: www.elsevier.com/locate/chroma

A numerical study of the assumptions underlying the calculation of the stationary zone mass transfer coefficient in the general plate height model of chromatography in two-dimensional pillar arrays

Daan De Wilde [a], Frederik Detobel [b], Johan Deconinck [a], Gert Desmet [b,*]

[a] Research Group Electrochemical and Surface Engineering, Department of Electro Technique and Energy Technique, Vrije Universiteit Brussel, Pleinlaan 2, 1050 Brussels, Belgium
[b] Department of Chemical Engineering, Vrije Universiteit Brussel, Pleinlaan 2, 1050 Brussels, Belgium

ARTICLE INFO

Article history:
Received 28 October 2009
Received in revised form 9 January 2010
Accepted 22 January 2010
Available online 29 January 2010

Keywords:
2D-Pillar array columns
Band broadening
C-term
Computational fluid dynamics
Mass transfer
Modeling

ABSTRACT

The present study investigates the validity of one of the key assumptions underlying the general plate height model of chromatography, i.e., the presumed independency of the individual band broadening contributions. More precisely, it is investigated under which conditions the mass transfer inside the stationary zone (e.g., porous pillars) is independent from the axial transport of species outside this zone, and how strongly any such dependency would affect the validity of the general plate height model of chromatography. For this purpose, detailed calculations of the species concentration distribution inside and outside the porous pillars of a computer-mimic of a porous pillar array column have been made. These simulations revealed a clear interplay between the mass transfer inside and outside the pillars, manifesting itself as an asymmetry of the species concentration distribution inside the pillars. The latter is in disagreement with the basic assumption used to calculate the value of the C_s-term of the general plate height model. The asymmetry-effect is largest at low reduced velocities, high retention factors and high intra-pillar diffusion coefficients. Fortunately, these are conditions where the C_s-term is relatively small, which might explain why the general plate height model of chromatography (and based on the symmetry assumption) can represent the band broadening in a porous pillar array within an accuracy on the order of some 1–2%.

1. Introduction

The band broadening in liquid chromatography (LC) columns is commonly modeled by assuming that it consists of four, independent contributions:

- the H_A-term contribution, representing the dispersive contributions originating from the erratic flow profile in the randomly shaped and sized through-pores of the packed bed media typically used in LC (so-called eddy-diffusion);
- the H_B-term contribution (=band broadening in absence of flow), arising from the mixed-mode molecular diffusion through the porous pillars and the interstitial void;
- the H_{Cm}-term contribution originating from the slow (radial) mass transfer in the mobile zone;
- the H_{Cs}-term contribution originating from the slow mass transfer in the stationary zone.

Because of the presumed independency of these different mass transfer processes, their contribution to the overall band broadening process can simply be added. The general expression for the band broadening (expressed in terms of the height of an equivalent theoretical plate) in packed chromatographic columns is therefore often written as [1,2]:

$$H = H_A + H_B + H_{Cm} + H_{Cs} \tag{1}$$

wherein H_A represents the eddy-dispersion contribution, which in the presently considered perfectly ordered porous pillar array can be theoretically described using a single term Giddings expression:

$$H_A = \left(\frac{1}{A} + \frac{1}{Dv_i}\right)^{-1} d_p \tag{2a}$$

The H_B-term in Eq. (1) represents the contribution of the effective longitudinal diffusion coefficient D_{eff}, and can be calculated as:

$$H_B = 2\frac{D_{eff}}{u_i}(1 + k'') \tag{2b}$$

wherein u_i is the average interstitial velocity and k'' is the zone retention factor. The physical meaning of the latter, as well the expressions for the two H_C-terms are discussed further on.

* Corresponding author. Tel.: +32 26293251; fax: +32 26293248.
E-mail address: gedesmet@vub.ac.be (G. Desmet).

0021-9673/$ – see front matter © 2010 Elsevier B.V. All rights reserved.
doi:10.1016/j.chroma.2010.01.070

The additivity of the different terms appearing in Eq. (1) has been discussed in great detail by Giddings [3]. Whereas the additive law has found widespread use, it should not be forgotten that Giddings also stated that the additive law is no longer correct as soon as there are two competitive mechanisms (with different rate parameters) contributing to the same mass transfer process. This is for example what led Giddings to his famous coupling theory to represent the eddy-dispersion, as he noted that this is an example of a band broadening process that results from two different and competing transport mechanisms (convection and diffusion). It should be remarked as a side-note that, with the notation adopted in Eq. (1), the Giddings coupling terms for the eddy-dispersion are incorporated in the expression for H_A (similar to the approach adopted in for example Eq. (37) of Ref. [1]).

Although Giddings warned that the independency of the individual terms of Eq. (1) should never be taken for granted, this advice has mostly been forgotten, most probably because the mathematics and the physical interpretation of Eq. (1) are so conveniently simple. And also because the complexity of the geometry wherein the different mass transfer processes have to compete in a packed bed of spheres is so complex that important rate parameters such as the intra-particle diffusion can not be determined with a perfect accuracy [4,5] so that Eq. (1) could never be put to a stringent accuracy test. With modern computation methods, using for example computational fluid dynamics (CFD) software or using Lattice–Boltzman methods [6,7], such stringent tests can nowadays be made. The combined power of modern computers and state-of-the-art commercial CFD software allows calculating the band broadening in systems with exactly known geometry and with exactly known local diffusion rates with an accuracy of about 0.1% [8].

Given the above, we found it worthwhile to reconsider the validity of Giddings additive law using such CFD methods, as there are a number of notable examples where this law is clearly not satisfied. One of the most notable examples perhaps is the band broadening in open-tubular LC or GC. The latter is described by the famous Golay–Aris equation [9,10], and it can be verified that this expression does not respect the additive law for what concerns the contribution of the velocity field and the species retention [3]. Another area where one would not immediately suspect a violation of the additive law is the B-term band broadening describing the longitudinal diffusion process. This process is usually modeled based on the assumption that the diffusion inside and outside the particles are independent processes so that their joint effect can be modeled using a (time-weighed) sum of the two individual contributions. However, as has been demonstrated in [4,5], the diffusion inside the particles cannot be treated independently from that outside the particles. This can readily be seen from the sketch in Fig. 1, showing that there are two competing diffusion processes that contribute to the process of diffusing from point A to point B (which is what the longitudinal diffusion process is all about). This can either occur by diffusing around the particle (trajectory 1) or by following the (usually slower) diffusion path through the particle (trajectory 2). The existence of these two trajectories implies there are two competing mass transfer mechanisms to ensure the longitudinal diffusion and this is sufficient to violate Gidding's general criterion for the validity of the addition law underlying Eq. (2).

Another reason why we found it worthwhile to reconsider the validity of the additive law is that the independency of the different mass transfer processes occurring in a column is also implicitly assumed in the general rate model, which is currently the most popular model used to analyze the individual band broadening processes of newly developed support formats such as monolithic columns and porous shell particles [11–16]. The general rate model, originally established and solved by Lapidus and Amundson [17] and Kucera [18], yields two relatively simple (and additive) expressions for the H_{Cm}-term and the H_{Cs}-term contributions to Eq. (1). These can generally be written as [2,19]:

$$H_{Cm} = 2\frac{k''^2}{(1+k'')^2}\frac{1}{\alpha Sh_{por}}\frac{\varepsilon}{1-\varepsilon}u_i\frac{d_p^2}{D_{mol}} \tag{3a}$$

$$H_{Cs} = 2\frac{k''}{(1+k'')^2}\frac{1}{\alpha Sh_{sz}}u_i\frac{d_p^2}{D_{sz}} \tag{3b}$$

wherein d_p is the characteristic thickness of the stationary zone (e.g., particle diameter in case of spherical particles), and wherein D_{mol} and D_{sz} are the molecular diffusion coefficients in respectively the mobile zone (liquid outside particles or pillars) and the stationary zone (intra-particle volume accessible to analytes). The zone retention factor k'', which emerges automatically when solving the general rate model, is related to the more customarily employed phase retention factor k' (which is defined with respect to the linear chromatographic velocity u_0) via:

$$k'' = (1+k')\frac{\varepsilon_T}{\varepsilon} - 1 \tag{4}$$

wherein ε is the external column porosity and ε_T is the total column porosity.

In Eq. (3), Sh_{por} and Sh_{sz} respectively represent the dimensionless mass transfer coefficient in the mobile and the stationary zone, i.e., they are film mass transfer coefficients [11,17–20] that have been multiplied by the pillar diameter and divided by the diffusion coefficient to obtain a dimensionless parameter. It can be shown [2] that Sh_{sz} is independent of the velocity (reflecting the absence of flow inside the pillars), and its value can be calculated analytically for a number of simple geometries, yielding for example $Sh_{sz} = 10$ for spherical particles and $Sh_{sz} = 8$ for cylindrical pillars. The mobile zone mass transfer coefficient (Sh_{por}) on the other hand is more dif-

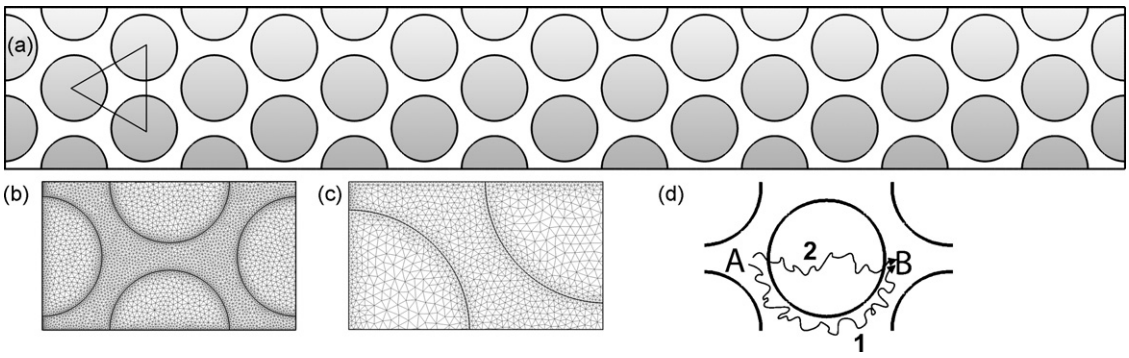

Fig. 1. (a) Top view of the considered packing geometry which is 2 unit cells high and 8 unit cells wide. The packing of the cylinders is based on an equilateral triangular arrangement. (b) Unit cell with grid. (c) Close up on the right top quarter of the unit cell to focus on the triangular grid that was used for all calculations. (d) Zoom-in on a single cylinder, showing two different trajectories that can be followed by a species molecule to travel from point A to B, as discussed in the text.

ficult to calculate, as the through-pore geometry is generally much more complex than the geometry of the particles or the pillars. In addition, it also depends in a yet unknown way on u_i. In [2,19] we have shown that Sh_{por} can best be represented using a two-term expression of the form:

$$Sh_{por} = \gamma_d + \gamma_c \nu_i^{1/3} \quad (5)$$

wherein γ_d and γ_c respectively represent the geometrical constant for the diffusive and the convective contribution to the mass transfer to the pillar surface in the flow-through-pores surrounding the pillars. It should be remarked that Eq. (5) reduces to the same form as that of the Wilson–Geankoplis or the penetration model [20] expression when γ_d is put to zero. The latter are two semi-empirical correlation that are commonly used to calculate the mass transfer in the through-pores of packed beds [11–16]. It was however our experience that the band broadening in ordered pillar arrays cannot be fitted appropriately without the addition of a γ_d-term [19]. The need for such a term is in our opinion a pure necessity, because its absence implies that the mass transfer would stop when the flow stops. This is clearly incorrect, because the mass transfer can still be maintained by pure diffusion if there is no flow.

The shape factor α appearing in Eq. (3) is proportional to the solid-volume based specific external surface Ω/V_{sz}, and is made dimensionless by multiplying it with a characteristic size (the diameter d_p of a spherical or cylindrical particle for example). For the case of cylindrical micro-pillars with diameter d_p, the definition of α results into $\alpha = 4$ ($\alpha = 6$ for spherical particles).

$$\alpha = \frac{\Omega}{V_{sz}} d_p = \frac{\pi l d_p}{\pi/4 d_p^2 l} d_p = 4 \quad (6)$$

In Eq. (6), l represents the height of the cylinders (l is infinitely large in the presently considered 2D geometry).

Despite the sound mathematical basis of the general rate model, it remains a given fact that it is also based on the presumed independency of the different mass transfer contributions. One of the clearest examples of this presumed independency is the form of the H_{Cs}-term expression given in Eq. (3b). This expression is directly based on the assumption that the concentration distribution around the pillars has a perfect spherical or cylindrical symmetry. That is, it is assumed that the concentration distribution around the pillars is perfectly concentric (angular symmetry), independently of the magnitude of the other mass transfer processes. Indeed, looking into the details of the general rate model (see e.g., Ref. [17]), it can clearly be noted that the differential equation expressing the intra-pillar transport only involves the radial coordinate (the angle coordinate is absent because of the presumed symmetry). Obviously, the concentration profiles ensuing from this type of cylindrical or spherical symmetry calculations can only be concentric. This same angular symmetry is also assumed in the H_{Cs}-term calculation procedure proposed by Giddings [3].

Returning to Fig. 1d, it can however readily be noted that the cylindrical or spherical symmetry assumption is only valid if the transport outside the pillars (combination of convection and diffusion) occurs much faster than that inside the pillars, so that the transport inside the pillars is independent from that outside the pillars. If the exterior transport is not infinitely fast, one again encounters a situation wherein a given mass transfer process (transport from A to B) can proceed along two competitive routes: one purely intra-pillar diffusion route (trajectory 1), and one exterior route where both convective and diffusive transport prevails (trajectory 2). According to Giddings' rule for the validity of the additive law, the existence of two competing processes again points at the fact that the simple additivity of a H_{Cs}-term of the form shown in Eq. (3b) might be invalid. In their 2006-paper, Gritti and Guiochon already rightfully acknowledged this (see comment to Eq. (53) of that reference), but the solution they suggested, i.e., the inclusion of a fudge factor F_{trans}, has found little resonance and was not fully elaborated.

Given the above, the present study has been set up to explicitly investigate the validity of the additive law assumption for the H_{Cs}-term as given by Eq. (3b). This validity has been investigated by calculating the species concentration distribution inside and outside the porous pillars of a computer-mimic of a porous pillar array column using a commercial CFD-package. Studying the band broadening in perfectly ordered systems provides the purest possible view on the H_{Cs}-term contribution, as its effect is not obscured by the eddy-dispersion strongly dominating the band broadening in real packed bed columns. Furthermore, since all results are obtained *in silico*, all system parameters (e.g., the mobile zone and the intra-pillar diffusion coefficient) are exactly known as they can be directly imposed by the user when defining the simulation problem. Another advantage of the adopted approach is the ease with which the mass transfer processes and the formed concentration gradients can be visualized.

Since the general plate height model of chromatography (cf. Eqs. (1) and (3)) has been established without making any a priory assumption about the degree of order or the dimension of the system (2D versus 3D), and since also the conditions underlying the validity of the additive rule are independent of the degree of order and the dimensions of the chromatographic bed, the general insights obtained in the present study should also apply qualitatively to all real packed column systems.

2. Considered geometries and employed numerical methods

Fig. 1 shows the general lay-out of the considered 2D geometry (top view), as well as the computational grid used to solve the general convection-diffusion mass balances. To generate a maximal isotropicity, the micro-pillars were positioned on the grid points of an equilateral triangular grid, with sides z ($z = 1.2294 d_p$ [21]) selected such that the total pillar volume exactly makes up 60% of the total bed volume, so as to yield a chromatographic bed with an external porosity of exactly $\varepsilon = 0.40$. The flow domain consisted of 8 consecutive unit cells in the x-direction and 2 unit cells in the y-direction. The global domain was then divided in about 130,000 grid cells.

The set of partial differential equations determining the flow field and the species dispersion was solved using an in-house developed software package [22,23] using a combination of finite element and residual approaches, the details of which have already been described elsewhere [6]. In short, a combined finite element and residual approach are used to solve the incompressible Navier–Stokes equations for a Newtonian fluid [6], combined with an extra force term (Lorentz force) if considering the case of electro-osmotic flows [24–27]. The flow field was calculated by imposing a given constant velocity at the inlet plane while a reference pressure was applied as the boundary condition at the outlet plane of the geometry. The lateral planes were subjected to a symmetry boundary condition.

The accuracy of the employed solver has been demonstrated in [6,28], where the plate heights calculated in a flow between two parallel stationary zone plates with gap d agreed to within 0.1% with the existing analytical solution. To achieve this accuracy, several grid sizes and time steps were used and compared with the analytical solution. The 0.1% accuracy was obtained in the case for which a further decrease in the calculation grid size and a further increase in the number of time steps no longer changed the result. The same grid size and time step independency was ensured when investigating the more complex geometry of the cylindrical pillar array case.

Hence, the reported result is obtained under conditions of maximal accuracy. Furthermore, since we use our own developed solver routine, which is optimized to solve this kind of problems in a very performant manner, we even refined the grid size and increased the amount of time steps beyond this point, as the computational cost was already reduced to a minimum by the optimized solver framework. Another confirmation for the accuracy of the numerical simulations was that the first order moment, corresponding to the mean residence time of the species, corresponded exactly (to within 0.02%) to the expected value based on the imposed values for the interstitial velocity and k''.

3. Results and discussion

3.1. Fitting quality of the general plate height model

Fig. 2 shows how the plate height curves for the two different considered values of the intra-pillar diffusion coefficient:

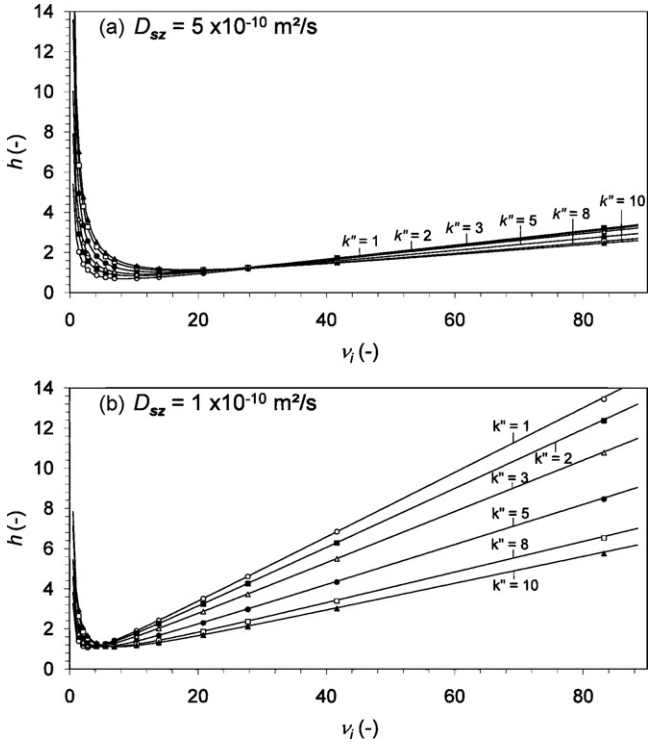

Fig. 2. Reduced van Deemter plot for (a) $D_{sz} = 5 \times 10^{-10}$ m^2 s^{-1} and (b) $D_{sz} = 1 \times 10^{-10}$ m^2 s^{-1} and for different values of k'': $k'' = 1$ (○), $k'' = 2$ (■), $k'' = 3$ (△), $k'' = 5$ (●), $k'' = 8$ (□) and $k'' = 10$ (▲). The solid lines were obtained by fitting the geometrical parameters (leading to $A = 0.021$, $D = 0.03$, $\gamma_c = 6.42$ and $\gamma_d = 4.2$) appearing in Eqs. (2a) and (5) to all the computed data points ($D_{sz} = 5 \times 10^{-10}$ m^2 s^{-1} and 1×10^{-10} m^2 s^{-1}-cases are fitted simultaneously). The value for Sh_{sz} was kept constant at its theoretical value ($Sh_{sz} = 8$) and D_{eff} was taken from independent measurements of the band broadening in the absence of convection (see Table 1 for the exact values).

Table 1
Calculated value of the effective diffusion coefficient D_{eff} (x10^{-10} m^2 s^{-1}), derived from peak-parking simulations for every considered combination of the molecular diffusion coefficient D_m, intra-pillar diffusion coefficient D_{sz} and zone retention factor k″ (all data relate to a mobile phase diffusion coefficient $D_{mol} = 1 \times 10^{-9}$ (m^2 s^{-1}). In the case of non porous pillars, there is no intra-pillar diffusion and k″ equals zero. In this case, D_{eff} is 6.21×10^{-10} m^2 s^{-1}.

D_{sz} (m^2 s^{-1})	k″					
	1	2	3	5	8	10
5×10^{-10}	6.70	6.55	6.25	5.64	4.81	4.45
1×10^{-10}	3.95	3.09	2.81	2.24	1.96	1.77

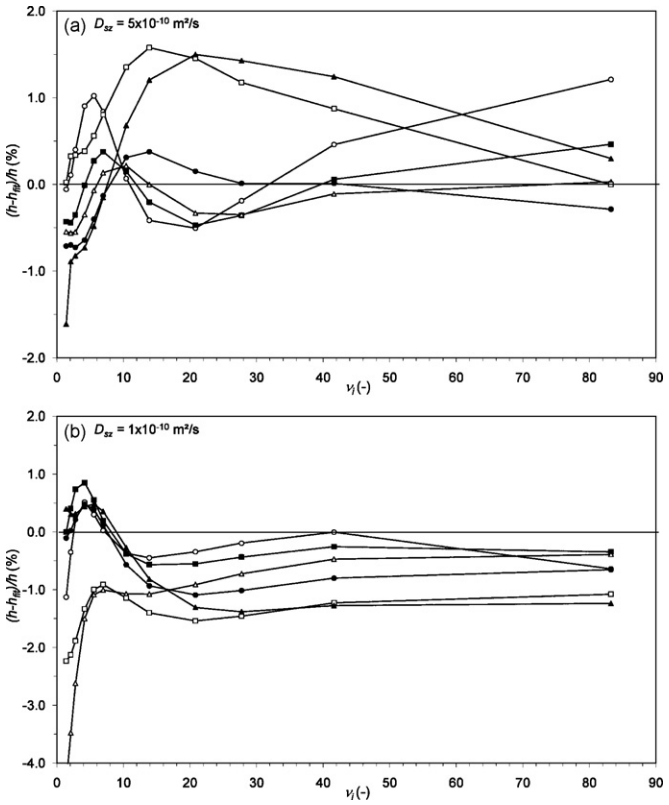

Fig. 3. Residual plots of the fitting shown in Fig. 2 (parameters fitted by considering the data series for $D_{sz} = 5 \times 10^{-10}$ m^2 s^{-1} and $D_{sz} = 1 \times 10^{-10}$ m^2 s^{-1} simultaneously). Same legend key as in Fig. 2.

$D_{sz} = 5 \times 10^{-10}$ m^2 s^{-1} (Fig. 2a) and $D_{sz} = 1 \times 10^{-10}$ m^2 s^{-1} (Fig. 2b) vary as a function of the velocity and the zone retention factor. As is customary in the field of LC, the data have been represented in the dimensionless format of $h = H/d_p$ versus $\nu_i = u_i d_p / D_{mol}$. The obtained h versus ν_i curves obviously depend very strongly on the value of D_{sz} and, in the low D_{sz}-case, also on the value of k''. This has already been discussed in great detail in [28] and is similar to that observed in a sister study [19], where the band broadening in perfectly ordered 3D structures was investigated. In short, this strong dependency is due to the exceptionally strong contribution of the H_{Cm}- and H_{Cs}-term compared to packed bed columns.

The full lines in Fig. 2 represent the best fit lines with Eq. (2), obtained using the values of k'' and D_{sz} that were used in the simulations to calculate the expressions for H_{Cm} and H_{Cs}, and using one set of best fit values for the A-, D-, γ_d and γ_c-constants (which are all plain geometrical constants). The fitting of these constants was conducted by considering the different (h,ν)-curves for the different cases of k'' and D_{sz} (12 in total) simultaneously and using the total sum of squares of the relative fitting error as the goal function of the fitting routine of the Solver add-in of MS® Excel (see figure caption for the resulting best fit values).

As can be noted from Fig. 2, the general plate height model defined by Eqs. (1) and (3) fits the computed plate height data remarkably well [28]. A similar fitting accuracy was observed in a sister study [19], conducting band broadening simulations in a perfectly ordered 3D geometry. The overall excellent fit between the general plate height model and the computed plate height data can in one sense also be considered as a validation of the employed (in-house developed) numerical computation schemes.

However, analyzing the fitting quality in greater detail by plotting the relative fitting residuals as a function of ν_i (Fig. 3), it can be observed that the fitting errors are not random but display

some systematic trends. These fitting errors therefore might point at some shortcomings of the general plate height model and the underlying additive law. At some particular values (mainly around $\nu_{i,opt}$) deviations of the order of 1–2% are observed. In real columns, fitting residuals of this order of magnitude would be considered as falling within the measurement accuracy limit, but the CFD calculations offer a much larger accuracy (order of 0.1% in the accuracy check with the analytical solution for the parallel plate channel system [6]) so that the deviations observed in Fig. 3 should be considered significant. These deviations are clearly systematic and not random, implying that they point at an intrinsic inability of the general plate height model to exactly represent all the subtleties of the band broadening process.

Interesting to note is that the absolute fitting residuals systematically go through a maximum around $\nu_{i,opt}$, i.e., around the minimum of the plate height curve (please note from Fig. 2 that $\nu_{i,opt}$ varies with k'' for the cases shown in Fig. 3a, whereas $\nu_{i,opt}$ remains around $\nu_i = 5$ for the cases shown in Fig. 3b). The other main general observation we can make is that the fitting errors of the $D_{sz} = 5 \times 10^{-10}$ m^2 s^{-1}-case are somewhat larger than in the $D_{sz} = 1 \times 10^{-10}$ m^2 s^{-1}-case, especially for the $k'' = 8$- and the $k'' = 10$-cases (solid triangles and open squares).

3.2. Detailed study of the intra-pillar concentration profiles

We subsequently investigated whether these systematic deviations can be linked to any deviation from the angular symmetry assumption underlying the expression for the H_{Cs}-term given by Eq. (3b). CFD simulations are ideally suited for this purpose, as the post-processing part of the simulation software allows making animated representations of how the species concentration distribution transforms as it makes its way through the flow-through-pores and the meso-porous pillars. These animations can be viewed while reading the online version of the manuscript and are also available as supplementary material (Mov_k2_Dsz_1_Pe3-15-60, Mov_k2_Dsz_5_Pe3-15-60, Mov_Pe15_Dsz_1_k2-5-10 and Mov_Pe15_Dsz_5_k2-5-10). When studying the movies, please note that the colour scale is constantly updated as the band moves through the column to maintain a maximal colour resolution (red = highest concentration at that moment, blue = lowest concentration at that moment). Here we only discuss one video frame selected from each movie (see Fig. 4a, b, etc.). For all cases represented in Figs. 4–7, this frame has been taken at the time at which the center of mass of the peak is positioned exactly in the middle of the represented flow geometry.

Fig. 4 shows how the concentration profiles (top view) depend on the flow rate (quantified here via the dimensionless ν_i-number) for a fixed value of k'' and D_{sz} ($k'' = 2$ and $D_{sz} = 1 \times 10^{-10}$ m^2 s^{-1}). As can clearly be noted, the concentration profile inside the individual pillars varies from strongly asymmetric at low ν_i to nearly perfectly symmetrical (i.e., concentric) at high ν_i. This change in symmetry can easily be understood as follows. At high ν_i, the transport around the pillars is sufficiently fast to rapidly bring the species from the upstream front of the pillars to the rear of the pillars before a significant amount of species starts to enter the pillars. As such, the species concentration is distributed evenly around the individual pillars, leading to a nearly perfect angular symmetry of the concentration at the pillar boundaries. Considering on the other hand the low ν_i-case ($\nu_i = 3$), it can clearly be noted that the convective transport along the pillars is in this case not fast enough to completely suppress the diffusion path through the pillars. As a consequence, a strongly asymmetric concentration profile is obtained. Similar asymmetric concentration profiles have already been reported under perfusive flow conditions in capillary electrochromatography [29].

Because of this asymmetry, we can expect that the Sh_{sz}-value appearing in the H_{Cs}-term will no longer be given by $Sh_{sz} = 8$, because the latter value is obtained under the strict assumption of an angular symmetry of the concentration boundary conditions (see Section 1). Since the degree of asymmetry changes with the ν_i-number, it can furthermore be inferred that the value Sh_{sz} is not even a constant, as assumed in Eq. (3b), but will vary with ν_i in the small ν_i-range.

Since the angular symmetry conditions leading to Eq. (3b) are clearly not satisfied in the low ν_i-range, we can now better understand the non-perfect fit between the general plate height model and the computed CFD data observed in Fig. 3. Since the assumption of a constant $Sh_{sz} = 8$-value appearing in Eq. (3b) is intrinsically wrong at low ν_i (the $Sh_{sz} = 8$-value only holds for the case of a mass transfer process with angular symmetry), one can simply not expect that the 4-term expression given by Eq. (1), with H_{Cs} given Eq. (3b), is able to fit the numerically computed data. However, trying to improve the model by accounting for the asymmetry in the boundary conditions of the concentration profile in the pillars at low ν_i seems very difficult, as it requires the introduction of the angular coordinate as an extra space dimension. This in turn increases the dimension of the set of partial differential equations that need to be solved, which inevitably leads to unwieldy mathematics.

The effect of the asymmetry of the boundary conditions on the Sh_{sz}-value can also be formulated in terms of Giddings' competitive transport mechanisms rule for the validity of the additive rule. As indicated by the arrows added to Fig. 4a, there are clearly two competitive routes along which species can be transported from point A to B: one convective/diffusive trajectory around the pillars, and one purely diffusive trajectory through the pillars. When ν_i is sufficiently large, the extra-pillar route is infinitely fast compared to the intra-pillar route, so that the competition between both routes is ruled out (in which case simply remains a constant) but when ν_i becomes sufficiently small (e.g., reaching the value of $\nu_i = 3$ as is the case in Fig. 4a) the two routes become competitive and start to influence each other, implying that the one contribution can no longer be calculated independently of the other.

The effect described here is similar to an effect described by Gritti and Guiochon [1], arguing that the axial transport inside and outside the porous particles of an HPLC column influence each other and suggesting a dependency between the diffusion through the particles and the axial dispersion (eddy-dispersion). Whereas these are most certainly also two band broadening sources that influence each other and can therefore not be simply added, the present study shows that the axial transport outside the porous particles also influences the value of the geometrical constant in the H_{Cs}-term, whereas this constant is usually considered as exactly known in many modeling studies [11,13–16,30].

Investigating now the effect of D_{sz} on the validity of the additive law and the accuracy of Eq. (3b) by plotting the concentration profiles for a larger D_{sz}-case than that considered in Fig. 4, it can be noted from Fig. 5 that the asymmetry-effect is in this case even more pronounced, as now even the $\nu_i = 60$-case still displays some asymmetry. This larger asymmetry is obviously in agreement with the higher intra-pillar transport rate. As a consequence, the transport inside the pillars can compete better with the transport outside the pillars, making it more difficult to achieve a perfect angular symmetry.

The larger asymmetry observed in the $D_{sz} = 5 \times 10^{-10}$ m^2 s^{-1}-case is of course also consistent with the fact that the $D_{sz} = 5 \times 10^{-10}$ m^2 s^{-1}-data series fit less well to the general plate height model than the $D_{sz} = 1 \times 10^{-10}$ m^2 s^{-1}-data, as can be noted from the differences in fitting quality between Fig. 3a and b. In the $D_{sz} = 1 \times 10^{-10}$ m^2 s^{-1}-case, the fitting residuals remain flat in the

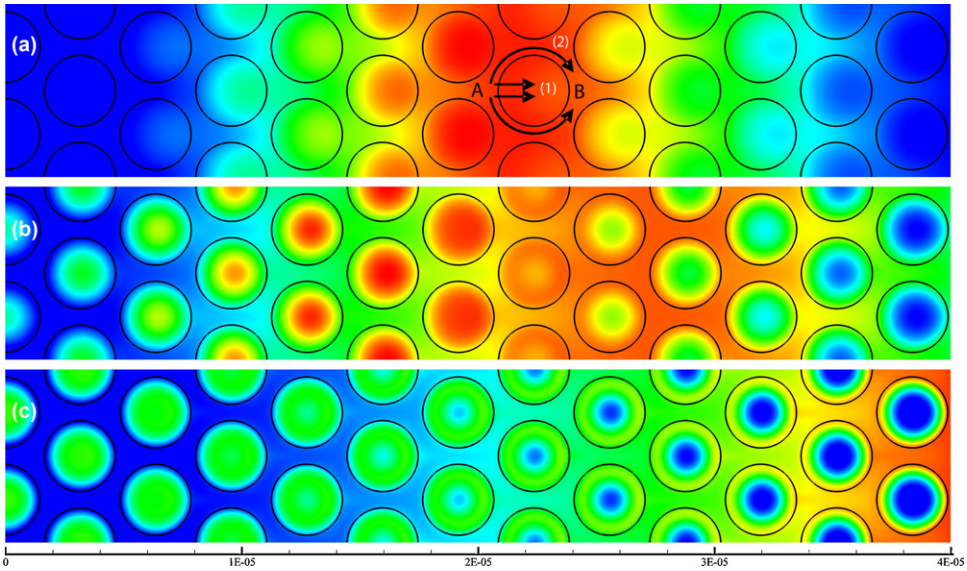

Fig. 4. Concentration distribution plots (top view) taken when the band has moved 20 μm downstream the pillar array for the case of $k'' = 2$ and $D_{sz} = 1 \times 10^{-10}$ m^2 s^{-1}, and for three cases of ν_i: (a) $\nu_i = 3$, (b) $\nu_i = 15$ and (c) $\nu_i = 60$. The two trajectory lines added to (a) represent two different transport paths that can be followed by a species molecule to travel from A to B, as discussed in the text.

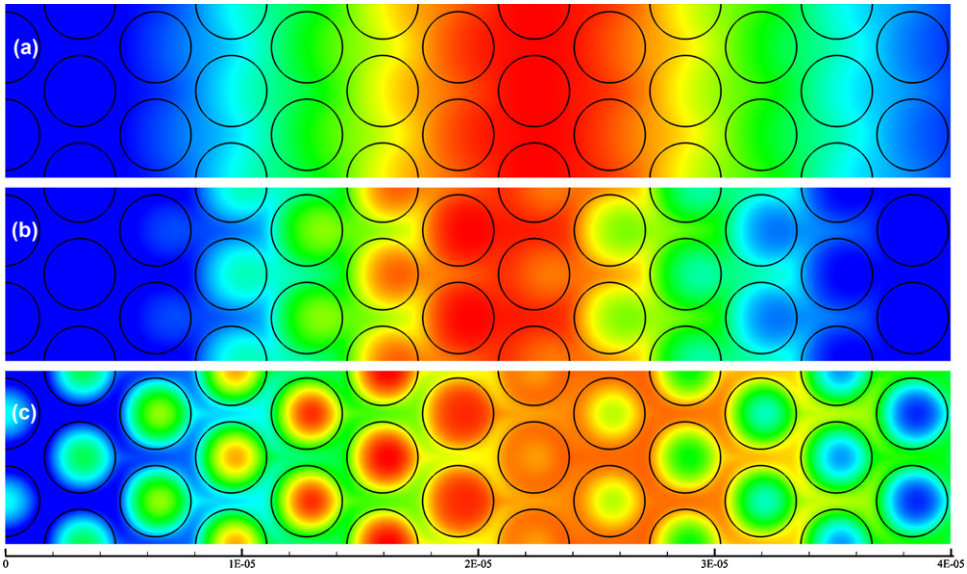

Fig. 5. Concentration distribution plots for the same conditions as shown in Fig. 4, except that $D_{sz} = 5 \times 10^{-10}$ m^2 s^{-1}.

large ν_i-range, where the angular symmetry of the concentration profile is nearly perfect. In the $D_{sz} = 5 \times 10^{-10}$ m^2 s^{-1}-case, the fitting residuals are forced into a more tortuous pattern. It is true that the fitting residuals in the $D_{sz} = 5 \times 10^{-10}$ m^2 s^{-1}-case also systematically deviate from 0, but this is due to the fact that the two cases were fitted simultaneously, so that inevitably the fitting error is "shared" between the two cases. When the $D_{sz} = 5 \times 10^{-10}$ m^2 s^{-1}- and the $D_{sz} = 1 \times 10^{-10}$ m^2 s^{-1}-case are fitted independently (see supplementary material), the $D_{sz} = 1 \times 10^{-10}$ m^2 s^{-1}-data series can clearly be much better fitted in the large ν_i-range (with residuals really tending towards zero), where the angular symmetry of the concentration profile is nearly perfect. This corroborates our hypothesis that the imperfect fitting of the computed CFD data is (at least partly) due to the interaction between the transport rates outside the pillars and the H_{Cs}-term, an interaction that is not accounted for by general plate height model. This interaction mainly occurs at low ν_i, and this is precisely the range where the fitting is at its worst in the $D_{sz} = 1 \times 10^{-10}$ m^2 s^{-1}-case. For the $D_{sz} = 5 \times 10^{-10}$ m^2 s^{-1}-case, the fitting residuals are high over the entire ν_i-range. In part, this can be considered as a reflection of the fact that the latter case is more prone to interactions between the intra- and the extra-pillar transport, and the enhanced asymmetry of the concentration profiles inside the pillars. It should however also not be forgotten that the dynamics of a multi-parameter fitting algorithm can be so complex that it not necessarily provides the best fit to the points where the model is most correct, so that the conclusion derived here above should not be overemphasized.

Figs. 6 and 7 show the effect of the zone retention factor k'' on the angular symmetry of the intra-pillar concentration profiles. As can be noted from Fig. 6 ($D_{sz} = 1 \times 10^{-10}$ m^2 s^{-1}-case), the asymmetry increases with increasing k''. This fully agrees with the fact that a larger k''-value implies that the species spend proportionally more time in the pillars, hence giving more prevalence to the (asymme-

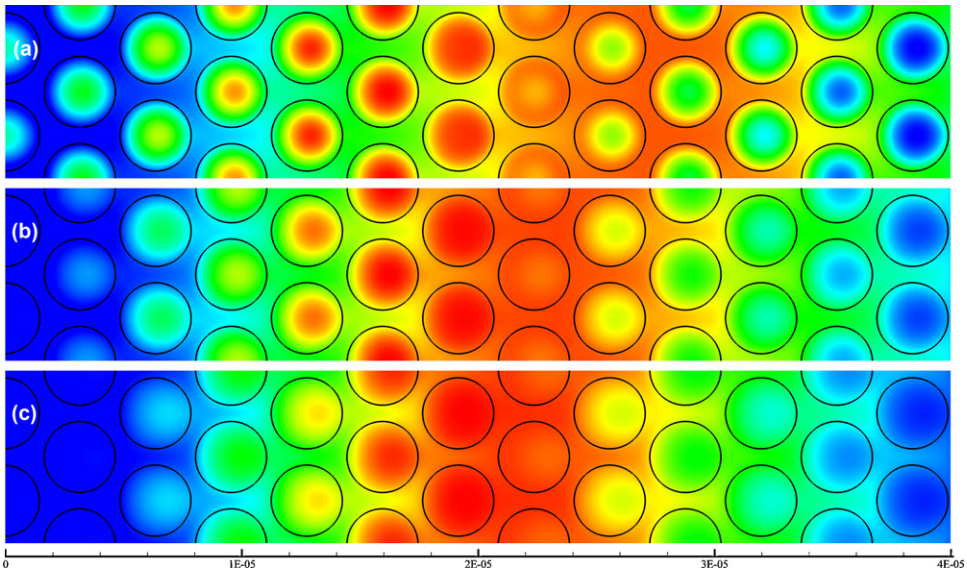

Fig. 6. Concentration distribution plots taken when the band has moved 20 μm downstream the pillar array for the case of $\nu_i = 15$ and $D_{sz} = 1 \times 10^{-10}$ m^2 s^{-1}, and for three cases of k'': (a) $k'' = 2$, (b) $k'' = 5$ and (c) $k'' = 10$.

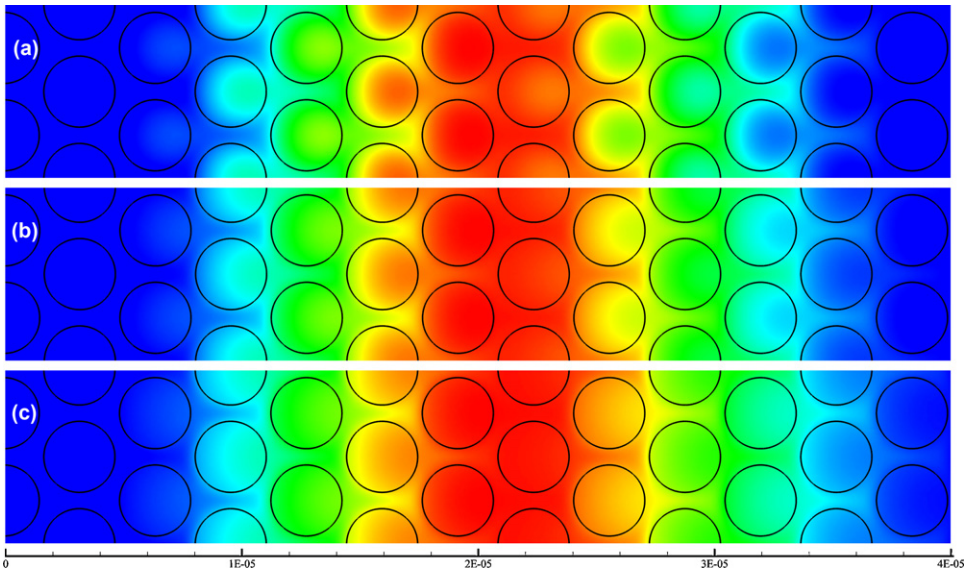

Fig. 7. Concentration distribution plots taken for the same conditions as in Fig. 6, except that $D_{sz} = 5 \times 10^{-10}$ m^2 s^{-1}.

try creating) intra-pillar transport route (cf. route 1 in Fig. 5a). The asymmetry enhancing effect of k'' is confirmed in Fig. 7, albeit now at a totally different level of overall asymmetry, as Fig. 7 relates to the $D_{sz} = 5 \times 10^{-10}$ m^2 s^{-1}-case for which the overall asymmetry is anyhow larger than for the case considered in Fig. 6.

Summarizing the above, it can be said that the angular symmetry underlying Eq. (3b) corresponds best to the physical reality for large ν_i, small k'' and small D_{sz}. Or put otherwise, the angular symmetry prevails if the transport rate outside the porous pillars occurs sufficiently faster than that inside the pillars. Cases where this angular symmetry is lost and wherein the species do not fill up or leave the pillars concentrically but rather axially can be expected to lead to a H_{Cs}-contribution that is no longer exactly given by Eq. (3b) with $Sh_{sz} = 8$ ($Sh_{sz} = 10$ in case of spherical particles). This is the case for systems with a high D_{sz} and/or a high k''. Fortunately, the H_{Cs}-term contribution becomes vanishingly small at high k'' (because of its $k''/(1 + k'')^2$-dependency), so that any inaccuracy of the H_{Cs}-term expression becomes less influential. The asymmetry becomes especially problematic at low ν_i, but the H_{Cs}-term contribution luckily also becomes vanishingly small in this range (especially if compared to the B-term contribution).

4. Conclusions

The well-established expression for the H_{Cs}-term band broadening contribution (cf. Eq. (3b)) is only valid when the species concentration distribution inside the pillars is perfectly concentric (i.e., has an angular symmetry). However, in cases with a low reduced velocity, a high retention factor and a high intra-pillar diffusion coefficient, the species fill up and leave the pillars rather axially instead of concentrically, leading to a severe deviation from the symmetry condition underlying Eq. (3b). The observed asymmetry can be considered as a manifestation of the fact that the mass transfer inside the stationary zone (e.g., porous particles or pillars) is not independent from the axial transport of species outside this zone. As a consequence, the basic rule underlying the addition of

the individual terms in the general plate height expression of LC (Eq. (1)) is violated.

In the present study, this has been observed by noting small, yet significant deviations a set of highly accurate plate height data (obtained in a highly ordered medium to minimize the obscuring effect of the eddy-dispersion) and Eq. (1). These deviations are most pronounced near the minimum of the plate height curve. Fortunately, the asymmetry in the concentration profiles in the particles (cylindrical pillars in the presently considered case) shows up under conditions where the C_s-term is relatively small, so that the fitting error remains very small (maximally some 1–2%), over a broad range of reduced velocities (up to $\nu_i = 90$) and retention factors (up to $k'' = 10$).

Nomenclature

A	Mechanical, diffusion independent, dispersion coefficient
D	Hydrodynamic, diffusion dependent, dispersion coefficient
D_{eff}	Effective diffusion coefficient ($m^2\ s^{-1}$)
D_{mol}	Diffusion coefficient in mobile zone (liquid outside particles or pillars) ($1.0e^{-9}\ m^2\ s^{-1}$)
D_{sz}	Diffusion coefficient in solid zone (intra-particle volume accessible to analytes) ($m^2\ s^{-1}$)
d_p	Pillar diameter (m)
H	Plate height (m)
H_A	Plate height originating from eddy-diffusion (m)
H_B	Plate height originating from longitudinal diffusion (m)
H_{Cm}	Plate height originating from mass transfer limitations in the mobile zone (m)
H_{Cs}	Plate height originating from mass transfer limitations in the stationary zone (m)
h	Reduced plate height, $h = H/d_p$
k'	Phase retention factor
k''	Zone retention factor
l	Height of the cylinders (m)
Sh_{por}	Sherwood number to express the mass transfer coefficient, k_{por}
Sh_{sz}	Sherwood number to express the mass transfer coefficient, k_{sz}
u_i	Average interstitial velocity ($m\ s^{-1}$)
V_{sz}	Volume of the stationary zone (m^3)

Greek symbols

α	Shape factor, $\alpha = 4$ for micropillars, $\alpha = 6$ for spherical particles
ε	External column porosity
ε_T	Total column porosity
γ_c	Geometrical constant representing the convective contribution to the mass transfer
γ_d	Geometrical constant representing the diffusive contribution to the mass transfer
ν_i	Reduced velocity or Peclet number, $\nu = ud_p/D_m$
Ω	Contact surface between mobile and stationary zone (m^2)

Acknowledgement

F.D. gratefully acknowledges a research grant from the Research Foundation – Flanders (FWO Vlaanderen). D. DW gratefully acknowledges the support from the HOA4 project funded by the Vrije Universiteit Brussel (HOA4-VUB).

Appendix A. Supplementary data

Supplementary data associated with this article can be found, in the online version, at doi:10.1016/j.chroma.2010.01.070.

References

[1] F. Gritti, G. Guiochon, Anal. Chem. 78 (2006) 5329.
[2] G. Desmet, K. Broeckhoven, Anal. Chem. 80 (2008) 8076.
[3] J.C. Giddings, Dynamics of Chromatography Part 1, Marcel Dekker, New York, 1965.
[4] G. Desmet, K. Broeckhoven, J. De Smet, G.V. Baron, P. Gzil, J. Chromatogr. A 1188 (2008) 71.
[5] K. Broeckhoven, D. Cabooter, F. Lynen, P. Sandra, G. Desmet, J. Chromatogr. A 1188 (2008) 189.
[6] D. Hlushkou, S. Khirevich, V. Apanasovich, A. Seidel-Morgenstern, U. Tallarek, Anal. Chem. 79 (2007) 113.
[7] S. Khirevich, A. Höltzel, A. Seidel-Morgenstern, U. Tallarek, Anal. Chem. 81 (2009) 7057.
[8] D. De Wilde, G. Weyns, N. Smets, P. Gzil, G. Desmet, J. Deconinck, Int. J. Comput. Methods 5 (4) (2008) 551.
[9] R. Aris, Proc. R. Soc. A 252 (1959) 538.
[10] M.J.E. Golay, in: D.H. Desty (Ed.), Gas Chromatography 1958, Butterworths, London, 1958, p. 36.
[11] F. Gritti, G. Guiochon, J. Chromatogr. A 1216 (2009) 4752.
[12] K. Miyabe, G. Guiochon, Anal. Chem. 72 (2000) 5162.
[13] K. Miyabe, G. Guiochon, J. Phys. Chem. B 106 (2002) 8898.
[14] K. Miyabe, J. Chromatogr. A 1183 (2008) 49.
[15] K. Kaczmarski, G. Guiochon, Anal. Chem. 79 (2007) 4648.
[16] K. Miyabe, M. Ando, N. Ando, G. Guiochon, J. Chromatogr. A 1210 (2008) 60.
[17] L. Lapidus, N.R. Amundson, J. Phys. Chem. 56 (1952) 984.
[18] E. Kucera, J. Chromatogr. 19 (1965) 237.
[19] F. Detobel, P. Gzil, G. Desmet, J. Sep. Sci. 32 (2009) 2707.
[20] K. Miyabe, Y. Matsumato, G. Guiochon, Anal. Chem. 79 (2007) 1970.
[21] P. Gzil, N. Vervoort, G.V. Baron, G. Desmet, Anal. Chem. 75 (2003) 6244.
[22] G. Nelissen, A. Van Theemsche, C. Dan, B. Van den Bossche, J. Deconinck, J. Electroanal. Chem. 563 (2) (2004) 213.
[23] L. Bortels, J. Deconinck, B. Van den Bossche, J. Electroanal. Chem. 404 (1) (1996) 15.
[24] R.F. Probstein, Physicochemical Hydrodynamics: An Introduction, 2nd ed., Wiley–Interscience, Hoboken, NJ, 1994.
[25] P. Attard, D. Antelmi, I. Larson, Langmuir 16 (4) (2000) 1542.
[26] E. Cummings, S. Griffiths, R. Nilson, P. Paul, Anal. Chem. 71 (11) (2000) 2526.
[27] A. Van Theemsche, J. Deconinck, L. Bortels, Electrochim. Acta 48 (20–24) (2003) 3307.
[28] D. De Wilde, F. Detobel, J. Billen, J. Deconinck, G. Desmet, J. Sep. Sci. 32 (23–24) (2010) 4077.
[29] U. Tallarek, M. Paces, E. Rapp, Electrophoresis 24 (2003) 4241.
[30] L. Hong, A. Felinger, K. Kaczmarski, G. Guiochon, Chem. Eng. Sci. 59 (2004) 3399.